PAPER • OPEN ACCESS

Electron emission from bromouracil and uracil induced by protons and radiosensitization

New Journal of Physics
The open access journal at the forefront of physics

Deutsche Physikalische Gesellschaft DPG
IOP Institute of Physics

Published in partnership with: Deutsche Physikalische Gesellschaft and the Institute of Physics

OPEN ACCESS

RECEIVED
4 March 2022

REVISED
5 June 2022

ACCEPTED FOR PUBLICATION
5 July 2022

PUBLISHED
21 July 2022

PAPER

Electron emission from bromouracil and uracil induced by protons and radiosensitization

Madhusree Roy Chowdhury[1,4], Juan M Monti[2], Deepankar Misra[1], Philippe F Weck[3], Roberto D Rivarola[2] and Lokesh C Tribedi[1,*]

[1] Tata Institute of Fundamental Research, Colaba, Mumbai 400005, India
[2] Instituto de Fisica Rosario, CONICET, Universidad Nacional de Rosario, 2000 Rosario, Argentina
[3] Sandia National Laboratories, Albuquerque, NM 87185, United States of America
[*] Author to whom any correspondence should be addressed.
[4] Present Address: Synchrotron SOLEIL, L'Orme des Merisiers, St. Aubin BP 48, 91192 Gif sur Yvette Cedex, France.

E-mail: lokesh@tifr.res.in and ltribedi@gmail.com

Keywords: electron spectroscopy, double differential cross section, radiosensitization, CDW-EIS, halouracils, forward–backward angular asymmetry

Abstract

Absolute double differential cross sections (DDCS) of electrons emitted from uracil and 5-bromouracil (BrU) in collisions with protons of energy 200 keV have been measured for various forward and backward emission angles over wide range of electron energies. The measured DDCS are compared with the continuum distorted wave-eikonal initial state (CDW-EIS) calculations. The optimized structure of the BrU was estimated along with the population analysis of all the occupied orbitals using a self-consistent field density. A comparison between the measured DDCS data for the two molecules show that the cross section of low energy electrons emitted from BrU is substantially larger than that for uracil. The BrU-to-uracil DDCS ratios obtained from the present measurements indicate an enhancement of the electron emission by a factor which is as large as 2.0 to 2.5. These electrons being the major agent for damaging the DNA/RNA of the malignant tissues, the present results are expected to provide an important input for the radiosensitization effect in hadron therapy. It is noteworthy to mention that the CDW-EIS calculations for Coulomb ionization cannot predict such enhancement. A large angular asymmetry is observed for uracil with a broad structure, which is absent in case of BrU.

1. Introduction

Studies on the interaction of ionizing radiations with biological matter has gained importance during the past few decades particularly due to its wide scale application for cancer treatment. The penetrating high energy beams of x-rays or gamma-ray photons, electrons and heavy-ions cause structural and chemical changes in the cells which eventually lead to cell death. When such radiation passes through the biological media, it leads to the generation of abundant low energy electrons. In addition, several hydroxyl radicals are also produced due to the interaction of the incoming beam with the surrounding water molecules, which comprises of about 60% of the weight of a human body. These low energy electrons and radicals are mainly responsible to damage the DNA/RNA of the cells by creating strand cleavages i.e., through single strand breaks (SSBs) and/or double strand breaks (DSBs) [1]. Thus the damage of the biological media caused by the incoming radiation is initiated by the elementary processes which take place at microscopic level in a very short time scale. The damage process is mostly related to the dissociation of the molecular constituents of the nucleobases. Further, it is well known that the ions possess preferential depth-dose profile while penetrating through the biological media compared to the photons which exhibit an exponential loss in intensity as it passes through the medium [2]. This unique feature of the high energy ions is well represented by the Bragg curve of energy loss which shows that ions deposit almost all of its energy at the end of the trajectory and with minimal energy transfer at the entrance of the track. Thus the deposition of the dose occurring precisely on the tumor, can be achieved by overlapping the position of the Bragg peak

with the tumor site. Protons are one of the most favourable candidates among the ions for damaging the tumors which has led to the development of several proton therapy centers worldwide.

Although high energy protons and carbon-ions are favourable candidates in hadron therapy yet a challenging task lies in the fact that many healthy cells which come along the particle track are also exposed to the ionizing radiation. To circumvent this difficulty, a complementary approach is being adopted which aims at increasing the sensitivity of the malignant cells to radiotherapy compared to the surrounding healthy cells. This radiosensitization effect which when combined with the proton therapy can serve as an effective mode of cancer treatment. The radiosensitizers when added to the tumors, results in the increase of electron production, which in turn not only enhances the reactivity of the malignant cells but also helps in reducing the dosage of the incoming beam, thus reducing the side effects to the healthy cells [3]. It has been proposed that the nanoparticles of gold, platinum and gadolinium can be useful candidates for radiosensitization [4]. Some of the experimental investigations have shown that the yield of SSBs and DSBs increase significantly when pure nanoparticles or nanoparticles coated with chelating agents are embedded to the DNA and are irradiated with photons, electrons or ions [5–7].

Similarly, the halouracils are also known to exhibit radiosensitizing properties [8–10]. These group of molecules ($C_4H_3XN_2O_2$) are structurally similar to uracil ($C_4H_4N_2O_2$), a nucleobase of RNA, except that the H-atom at the 5th position is replaced by a halogen (X = F, Cl, Br, I). Several experimental and theoretical studies have been carried out showing the different fragmentation channels from the isolated molecules of halouracils or hydrated clusters of halouracils irradiated by the photons, ions and electrons [11–17]. The studies on the dissociative electron attachment in case of few eV electrons impacting on 5-bromouracil (BrU) have also been reported [18]. The first study of the enhancement in electron emission from iodouracil and the influence of the atomic giant resonance has been reported recently [19] for higher energy [66 MeV C^{6+} ions] collisions.

The present work is divided into two parts. In the first part we have reported the absolute double differential cross sections (DDCS) of the electrons emitted from uracil and bromouracil induced by protons having energy 200 keV. Different experimental and theoretical studies on electron emission and fragmentation of uracil and other nucleobases, such as, adenine, cytosine, thymine in collisions with electrons, protons and heavy ions have been reported in the literature [20–32]. In case of simulating the proton trajectory [33] and for modelling its energy loss in biological medium, it is necessary to have an accurate estimation of the contributions from ionization, fragmentation and capture processes that occur during the collision. However, to the best of our knowledge no measurement exists on the DDCS of electron emission from BrU or other halouracils [except iodouracil [19]] when ionized by electrons or ions. In case of proton therapy, the incident beam energy vary around few hundreds of MeV. The present beam energy was chosen considering the fact that for such high energy protons, the position of the Bragg peak is around 100 keV [34]. The percentage of the DNA damage decreases with increase in beam energy and is maximum in the energy range of 100 to 200 keV. In the second part of the study, we provide a quantitative estimate of the enhancement in the electron emission from BrU. Such a quantitative study might serve as an input for estimating the reduction in dosage of the incident beam without altering the yield of SSBs and DSBs.

2. Experimental details

The experiments were performed in a crossed beam setup where the projectile beam collided with the vapour of uracil or bromouracil. The protons of energy 200 keV were generated from the 14.5 GHz 200 W electron cyclotron resonance (ECR) ion accelerator at TIFR, Mumbai [35–37]. The ECR ion accelerators are well known for producing the low velocity, highly charged ions. The positively charged ions were produced inside the Cu plasma chamber which is confined within a strong magnetic field of nearly 1 T. The ions were extracted by applying an extraction voltage of 30 kV and then a 90° bending dipole magnet was used to analyze the energy and charge state of the H^+ ions. The plasma chamber, Einzel lens and the bending magnet are all placed together on an isolated high voltage deck which can be biased up to 400 kV. The analyzing magnet is followed by an accelerating column. A few electrostatic triplet quadrupole lenses and X–Y deflectors are used to focus the energy and charge state analyzed projectile beam. The ECRIA has four beamlines with a switching magnet that steers the beam in the desired beamline. A pair of four-jaw slits were used to cut the beam and control its divergence. In addition, two apertures of diameter 2 mm and 4 mm were placed at the entrance of the scattering chamber for further beam collimation. A differential pumping station was connected between the beamline and the scattering chamber. The beamline vacuum was maintained at an absolute pressure of 5×10^{-9} mbar whereas that for the scattering chamber was at 10^{-8} mbar. The experiments were performed using the electron spectroscopy technique. A hemispherical electrostatic analyzer was used to measure the energy and angular distribution of the electrons emitted from

the target. Extreme cleanliness was maintained inside the chamber to reduce any stray field near the interaction region which could deflect the low energy electrons. The Earth's magnetic field was reduced to about 10 milligauss near the interaction region by attaching two sets of μ metal sheets at the inner walls of the scattering chamber. The entrance and exit slits of the spectrometer were biased with a small pre-acceleration voltage of 6 V, which increased the collection efficiency of the low energy electrons. The analyzed electrons were further detected by the channel electron multiplier (CEM), the front cone of which was raised to a positive potential of 100 V since the efficiency of the CEM remains constant between 100 and 600 eV when operating in electron counting mode.

The measurements for the uracil and bromouracil were carried out under the same experimental conditions. The commercially available powder of uracil or bromouracil (purity 99% and 98%, respectively) was placed in a metallic oven. For both the cases, the powders were heated gradually to about 190 °C over a period of 24 h which ensured it to be fully devoid of moisture. This temperature is far below the decomposition temperature of uracil and its halogenated derivatives [38]. The oven temperature was monitored by a thermocouple temperature sensor coupled to the heater body. The oven was housed inside a water cooled jacket to reduce the generation of dark counts. Further, it is extremely important to obtain a steady flow of the vapour while performing the measurements. A quartz crystal based thickness monitor was used to check the rate of flow of the vapour effusing from the nozzle. The effusive beam of the molecules were ejected through the jet nozzle of diameter 1.5 mm and length 12 mm. The tip of the nozzle was kept 5 mm below the beamline. The data were collected for ten different forward and backward emission angles between 20° and 150°. For either molecules, the background counts were very low. A LabVIEW based data acquisition system was used. The experimental uncertainties for the DDCS and TCS data for both the molecules varied between 24 and 28%.

In the same experiment, the absolute e-DDCS measurements were carried out for a much smaller molecule, like, CH_4 under static gas pressure condition. The DDCS measurements for CH_4 was used to initially check the performance of the spectrometer. However, in case of experiments involving an effusive jet source (uracil and bromouracil), it is difficult to ascertain accurately the number density of the target molecules interacting with the projectile beam. A novel technique that is, using the K-LL Auger yield of carbon atoms in CH_4 and further in uracil and bromouracil was used for absolute normalization of the electron DDCS for the vapour targets [24].

3. Theoretical description

Theoretical calculations based on the CDW-EIS approximation has been discussed previously [19]. In brief, an independent particle approximation has been employed where the reaction is reduced to a one-active-electron process [39]. Thus each one of the electrons of the different molecular orbitals is promoted separately to a continuum state, whereas it is assumed that the rest of the target electrons remain in their initial states. The prior version of the CDW-EIS approximation, within the impact parameter approximation, is employed to describe the reaction [40].

In order to describe the initial orbital plane-wave function, each molecular orbital was expressed as a linear combination of the atomic orbitals (LCAO) using *ab initio* calculations. Figure 1 shows a ball-and-stick representation of the optimized ground-state structure of the 5-bromouracil molecule. The atoms are labeled with numbers that allow to individually identify them in the different molecular orbital representations. *Ab initio* calculations were carried out for an isolated 5-bromouracil molecule using the restricted Hartree–Fock method implemented in the Gaussian 09 software [41]. The C, H, O, N, and Br atoms were represented using Pople's split-valence triple-zeta basis set 6-311G. The first ionization energy calculated using Koopmans' theorem at this level of theory is 9.93 eV. This predicted value for bromouracil appears slightly larger than the corresponding uracil experimental values of 9.8 $\pm$ 0.1 eV measured by Lifschitz *et al* (electron impact) [42] and 9.68 eV obtained from photoelectron spectroscopy (vertical value) by Palmer and coworkers [43].

The optimized structure of the 5-bromouracil molecule adopts the C_s point-group symmetry, without symmetry constraint applied in the relaxation calculation. A population analysis of all occupied orbitals was carried out using the self-consistent field (SCF) density, with the minimum contribution percentage to include in individual orbital population analysis set to 1%. For each j-molecular orbital, the effective number of $\xi_{j,i}$ electrons, relative to the atomic component i, was obtained from a standard Mulliken population analysis. The ionization energies, the atomic components with their corresponding nl states, for each one of the 46 molecular orbitals are calculated along with the population of the different components (not shown).

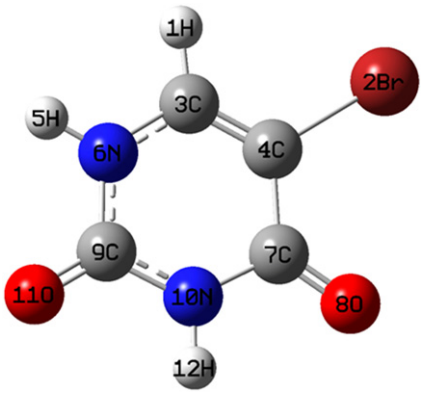

Figure 1. Ball-and-stick representation of the optimized ground-state structure of the 5-bromouracil molecule (C_s point-group symmetry).

4. Results and discussions

4.1. DDCS: energy distribution

In figure 2 we have shown the absolute electron DDCS for uracil (blue open triangles) and bromouracil (black open circles) at various forward and backward emission angles. The DDCS spectra are seen to fall by orders of magnitude in the measured energy range from few eV to several hundreds of eV, which is a typical behaviour in ion-atom collisions. A hump like structure is observed around 350 and 200 eV for the emission angles 20° and 45°, respectively (see figures 2(a) and (b)). The hump is due to the binary encounter mechanism between the projectile and the target electron. Three peaks are observed at the backward angles, overriding on the continuum Coulomb ionization background which are due to the K-LL Auger electrons emitted from C, N and O atoms, respectively. The insets of figure 2(f) show the magnified view of the three K-LL Auger peaks after subtracting the Coulomb ionization background. Panel (i) shows the K-LL Auger peak of C atoms whereas panel (ii) shows the same for N and O atoms. These Auger peaks are not observed for the forward angles since they are submerged under the strong continuum background spectrum arising from the binary encounter process. The measured DDCS spectra for uracil and BrU are seen to almost merge with each other for the forward angles in the log-log scale. However, the difference between the cross sections increases for larger emission angles in the backward direction.

The experimentally obtained DDCS for both the molecular species have been compared with the CDW-EIS calculations. At small forward angles, the theoretical DDCS for uracil and BrU almost merge together over the entire emission energy range. With the increase in the emission angles, the difference between the CDW-EIS calculations for these two molecules show up only beyond 40 eV. Now, while comparing the measured data with the theoretical values it is seen that in case of 20°, the calculations for uracil underestimate the data below 280 eV, beyond which it matches with the data. Similarly, for bromouracil, the calculations underestimate the data over the entire spectrum although the difference decreases at higher emission energies. The hump observed in the experimental DDCS spectrum due to the binary collision is well reproduced by the CDW-EIS calculations. For 45° and 90°, the theoretical DDCS for both uracil and bromouracil are lower than the experimental data in the measured energy range although the difference is more in the case of BrU. For the backward angles, the measured DDCS for uracil is found to be in close agreement with the CDW-EIS calculations up to about 30 eV beyond which the model underestimate the experimental data. In the case of BrU, the CDW-EIS prediction underestimates the data for the backward angles with large discrepancies occurring at higher emission energies. The large discrepancy between the experimental data and calculations for the higher energy electrons at the backward angles is explained by the backscattering phenomena. The higher energy electrons are influenced by the backscattering produced by the target nuclei on the emitted electrons [44]. For bromouracil, although the CDW-EIS calculations show a qualitative agreement, quantitatively it underestimates the measured DDCS over the entire energy range for both the forward and backward angles.

4.2. DDCS: angular distribution

In this section we discuss the variation of the electron DDCS as a function of the ejection angles, as shown in figure 3. For all the energies it is observed that the cross section is maximum at the extreme forward angles and decreases gradually as the emission angle increases. The difference in the DDCS between low forward and large backward angles varies by one or two orders of magnitude for lower energies whereas for

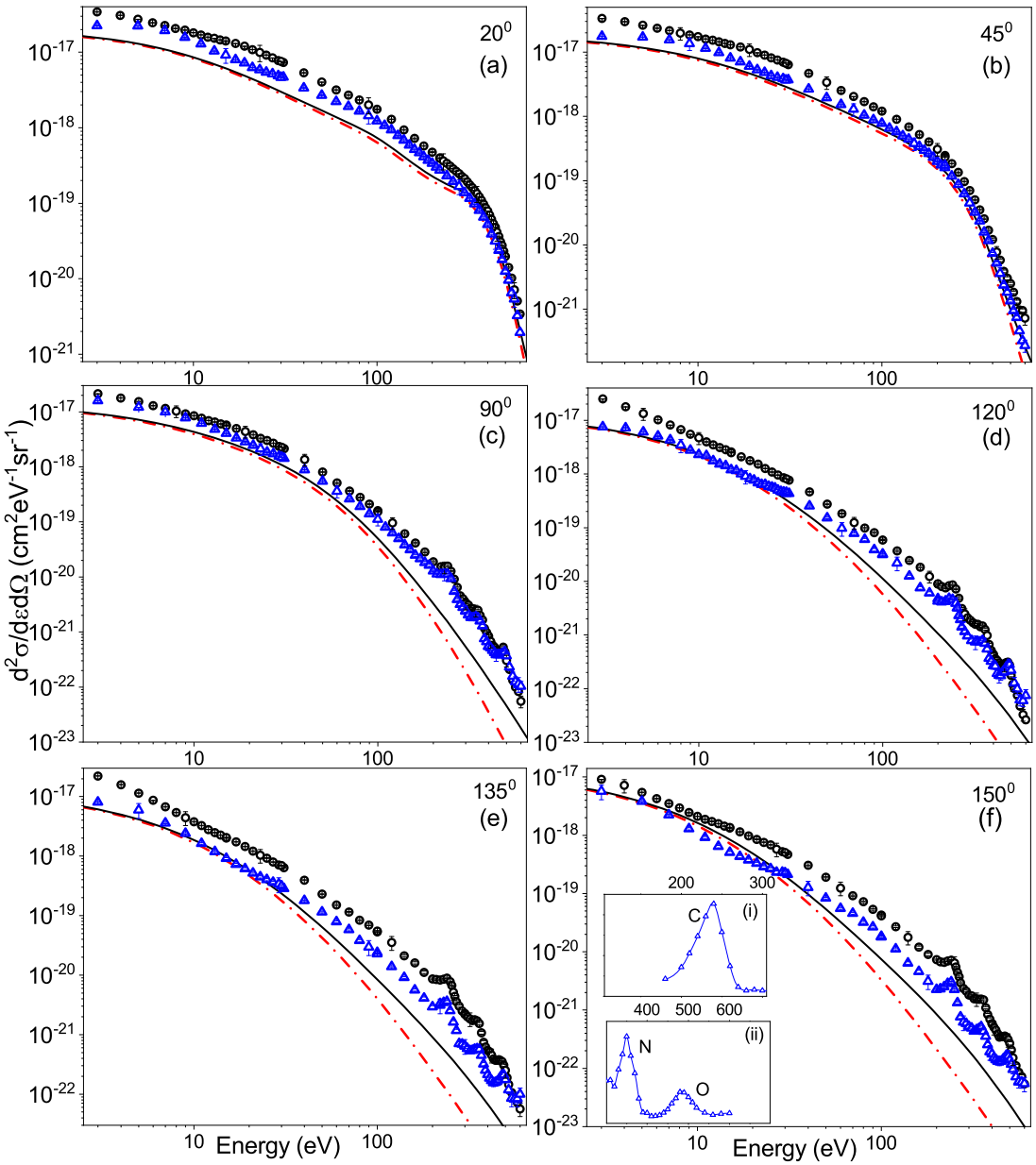

Figure 2. Absolute electron DDCS for BrU (black open circles) and uracil (blue open triangles). CDW-EIS calculations for BrU and uracil are shown by the black solid lines and red dashed lines, respectively. The absolute errors are shown for some of the data points whereas for the rest, the statistical uncertainties are displayed. Insets in (f): K-LL Auger peaks for C (panel (i)), N and O atoms (panel (ii)) in linear scale after background subtraction.

higher energies this difference increases even further. The large cross section in case of the forward angles may be explained by the strong two center (target and projectile) effect (TCE) and post collision interaction (PCI) between the moving projectile and the emitted electrons. In the present case, the projectile velocity is 2.82 a.u. which is closer to the orbital velocity of the valence electrons. Thus the projectile spends sufficient time close to the target and hence has a strong effect on the ionized electrons. The ejected electron experiences a strong pull along the direction of the moving positively charged projectile-ion which gives rise to the large DDCS in the low forward angles. The measured cross section shows an excellent agreement with the CDW-EIS calculations qualitatively. However, quantitatively it is seen that the model underestimates the data for both the molecules. For the low energy electrons, the difference between the experimental and theoretical DDCS remains the same over all the emission angles. The model underestimates the data by a factor of two to three. However, for higher electron energies, for example, in case of 200 eV, the CDW-EIS calculations for bromouracil are two times lower than the experimental data and this difference increases by almost an order of magnitude for the farthest emission angles due to the backscattering phenomena, as explained in the previous section. Similar behaviour is observed for the uracil molecule. Further, it is to be noted that there is no significant difference between the calculated DDCS for uracil and bromouracil for the

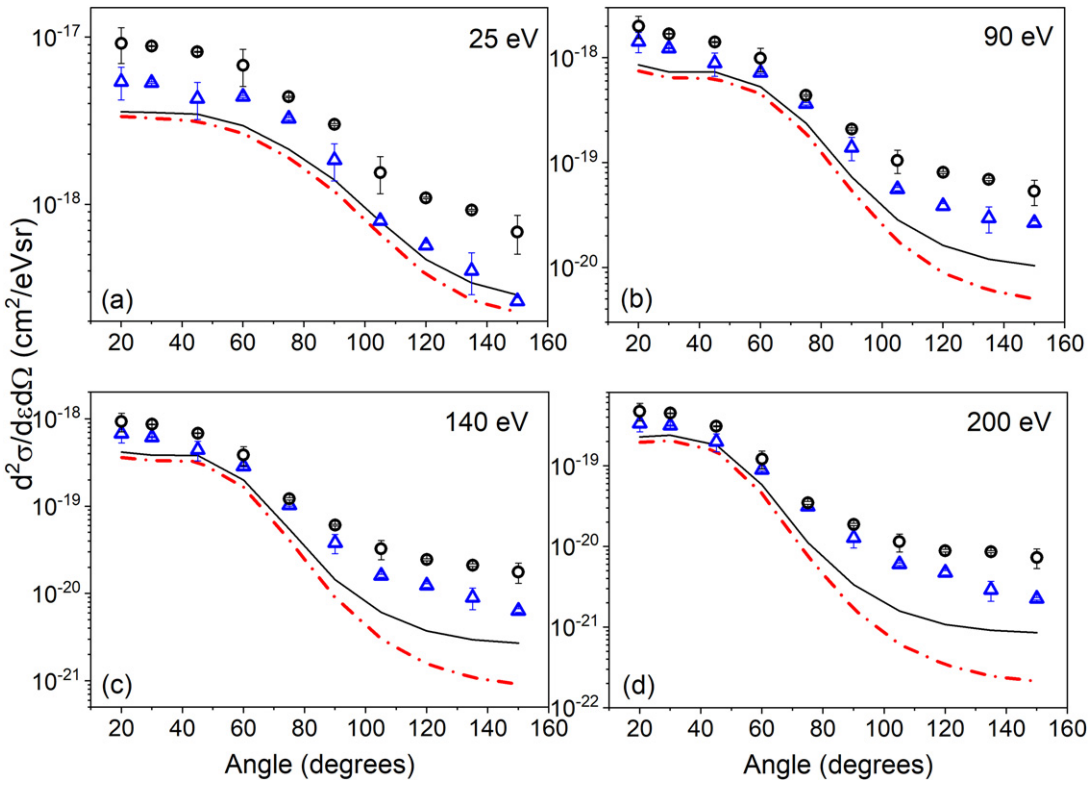

Figure 3. Experimental and theoretical e-DDCS of BrU and uracil as a function of emission angles. Legends are similar to those used in figure 2. Absolute error in the data are shown for few cases.

low energy electrons at all the emission angles. For higher electron energies, only beyond 80°, the DDCS for uracil is seen to be appreciably lower than that for BrU. However, the experimentally measured DDCS for BrU is seen to be uniformly higher than uracil for all the angles in case of low energy electrons. As the electron energy increases, i.e., beyond 50 eV, the difference in cross section between the two molecules is higher for the backward angles compared to the forward angles. This difference has been discussed in details in the following section.

4.3. DDCS ratios

Figure 4 shows the ratio of the DDCS for bromouracil to uracil over the electron energy range between 8 and 100 eV. These ratios have been plotted for four different emission angles. The DDCS ratio plots provide a quantitative estimate of the enhancement in electron emission from bromouracil compared to that for uracil. It is observed that in case of the forward angles, the experimental DDCS ratio varies between 1.5 and 1.75 whereas it increases at the backward angles. In case of the farthest backward angles i.e., for 135°, the experimentally obtained DDCS for BrU is about 2.25 times the cross section for uracil whereas for 150° the ratio goes as high as 2.5 times for electron energies between 15 and 30 eV. Beyond 30 eV the ratio is found to be around 2.3. The increase in ionization cross section in this electron energy range bears special importance due to its application in proton therapy. The DDCS ratio obtained from the CDW-EIS prediction (red solid lines) are seen to remain uniformly flat around 1.1 in case of the forward angles. For large backward angles, the CDW-EIS ratio is seen to remain about 1.1 till 40 eV, beyond which it increases gradually to 2.3 at 100 eV. A closer look at all the panels in figure 4 reveals a small structure in the DDCS ratios between 10 and 30 eV. These structures may arise due to the Coster–Kronig or super Coster–Kronig transitions in Br atom present in the bromouracil molecule which are reported in very recent experiments [45, 46]. Such mechanisms give rise to several low-intensity lines in the low energy electron spectrum which are not included in the CDW-EIS model. This partially explains the discrepancy with the model in the low energy region. Further, the low energy electrons are emitted predominantly due to the large impact parameter collisions where the projectile interacts ('sees') with the whole molecule. Therefore the calculated ratios are sensitive to the exact structure or wavefunctions used in the calculations for both the molecules.

Similarly, figure 5 displays the angular dependence of the DDCS ratios. In this block we have shown the ratio only for low energy electrons, such as, 11 and 30 eV since the electrons in this energy region play most crucial role for damaging the DNA/RNA strands. It is observed that the ratios remain the same i.e. around

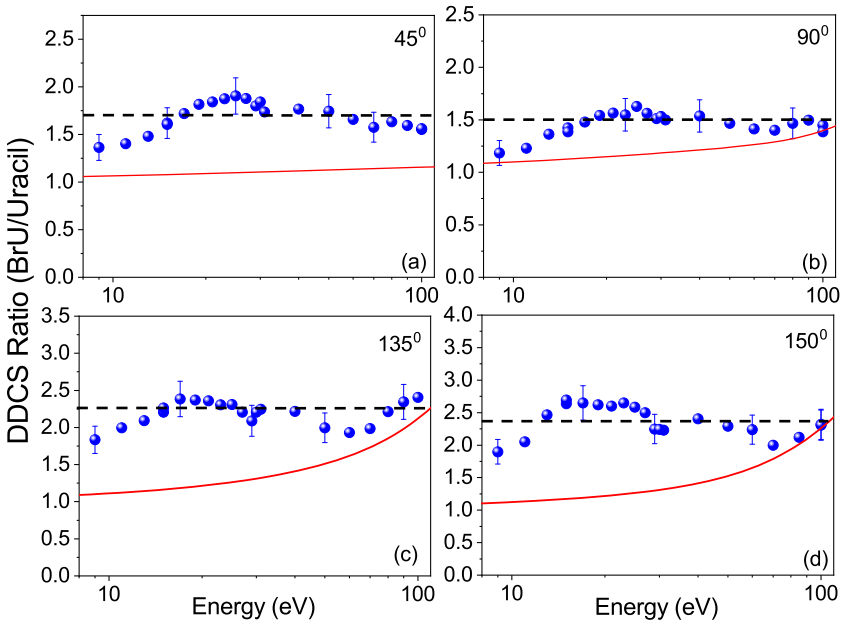

Figure 4. DDCS ratio of bromouracil to uracil as a function of electron energy. Error bars are shown for some of the data points. The red solid line shows the theoretical ratio. The black dashed line is guide to eye.

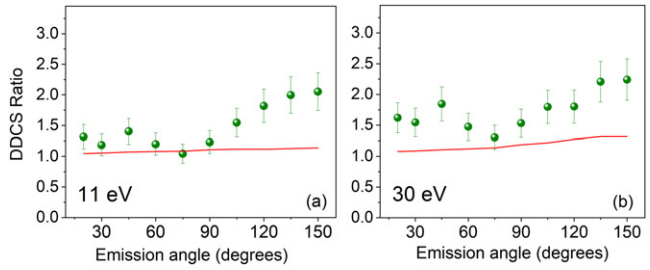

Figure 5. The ratio of BrU to uracil as function of emission angle along with the CDW-EIS calculations.

1.5 for the forward angles and then start increasing steadily to about 2.3–2.5 at 150°, the largest backward angle for which the spectrum has been measured. The CDW-EIS ratios (red solid lines) show a horizontal distribution about 1.1 over all the emission angles. The increase in the experimental DDCS ratio at the large backward angles arises from the influence of the nuclei on backscattering emission. The electron, in order to be emitted in the backward direction, must penetrate in the proximity of the nucleus. Thus, this process is dominated by a close interaction with the nucleus. In the case of BrU, a H atom is replaced by a Br atom, which has a much larger nuclear charge and thus the backward emission is enhanced in comparison to that for uracil.

The overall enhancement in the electron emission cross section from bromouracil compared to uracil (figures 4 and 5) may be explained by the Auger cascade effect as well as the atomic giant resonance phenomena. The vacancy created in the 3d shell of a Br atom gives rise to an Auger cascade and several electrons in the energy range between 40 and 50 eV [47] can be generated from the *MNN* Auger process. A part of these electrons may also be produced due to collective excitation which occurs when the 3d electrons are resonantly excited to higher excited states and finally decays by emission of several electrons. Such atomic giant resonance is not only well known for the 4d-elements, such as, I and Xe but also has been theoretically predicted for a 3d-atom, such as, Kr [48]. In Br compounds the information on collective effects are scarce, however, the giant shape resonance of $3d^{10}$ to $3d^{9}\epsilon f$ has been identified experimentally [49].

4.4. Forward backward angular asymmetry

From figure 3 it is already observed that there is a large asymmetry in the DDCS for the extreme forward and backward angles for both targets due to the strong PCIs apart from the non-Coulombic target potential. We provide a quantitative estimate of the angular asymmetry between the two supplementary

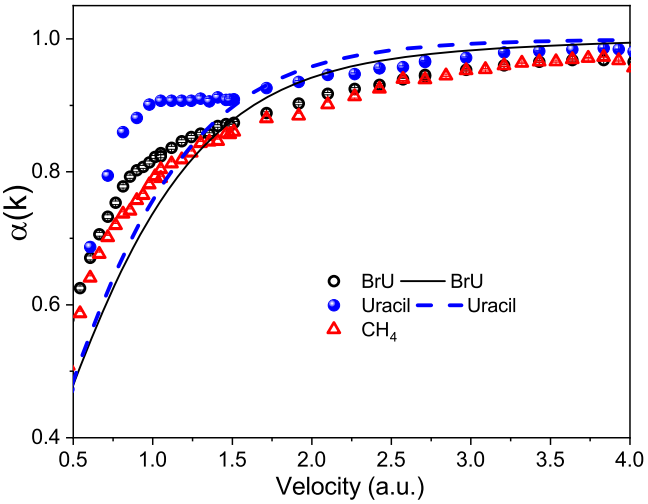

Figure 6. Forward backward angular asymmetry parameter ($\alpha(k)$) for uracil (blue sold circles) and bromouracil (black open circles) along with the lines corresponding to the CDW-EIS predictions. The red triangles correspond to $\alpha(k)$ for CH_4.

angles. The forward–backward angular asymmetry parameter ($\alpha(k)$) is defined as following: [50]:

$$\alpha(k,\theta) = \frac{\sigma(k,\theta) - \sigma(k,\pi-\theta)}{\sigma(k,\theta) + \sigma(k,\pi-\theta)}, \tag{1}$$

where the electron energy $\epsilon_k = \frac{k^2}{2}$ in a.u., θ is a low forward angle *and* k denotes the ejected electron velocity. In the present study, the $\sigma(k,\theta)$ and $\sigma(k,\pi-\theta)$ correspond to the electron DDCS measured at 30° and 150°, respectively. Using equation (1) we have calculated an approximate value of the asymmetry parameter ($\alpha(k)$). Figure 6 displays $\alpha(k)$ as a function of the ejected electron velocity for BrU and uracil. It is obvious that the $\alpha(k)$ is sensitive to the velocity (v_p), the charge state (q_p) of the projectile, the non-Coulombic potential of the target and its molecular wave function. The asymmetry parameter for BrU is seen to increase steadily from 0.6 to 0.9 corresponding to the electron velocities between 0.5 and 3.0 a.u. and beyond 3.0 a.u. $\alpha(k)$ shows a tendency to saturate. In case of uracil molecule, the overall angular asymmetry is higher than that for bromouracil. The black solid and blue dashed lines in figure 6 represent the $\alpha(k)$ obtained from the CDW-EIS calculations for BrU and uracil, respectively. Theoretically, the asymmetry parameter for both the biomolecules increase steadily from 0.5 to 0.99 up to the electron velocity of 2.75 a.u. beyond which both the curves tend to saturate. The unusually large asymmetry parameter obtained experimentally for uracil compared to that for BrU cannot be explained by the CDW-EIS model. Further, between 0.5 and 1.5 a.u., one can see a broad structure overriding on the steadily increasing $\alpha(k)$ for the uracil molecule. It is noteworthy to mention that the broad structure is observed only in the case of uracil but not for the BrU. Further investigations along with theoretical calculations are required for the precise explanation of the structure in uracil which is beyond the scope of this work. In order to explore this in more detail, we have obtained the asymmetry parameter for a smaller molecule, CH_4 (red open triangles). The asymmetry ($\alpha(k)$) for CH_4 is seen to increase monotonically and is lower than that for BrU up to 2.25 a.u. beyond which it completely merges with that of BrU. The asymmetry parameter trend seen for bromouracil is quite similar to that usually observed for ion collisions with atoms or small molecules.

Integration of the DDCS over the emission energy and the angle yields the total ionization cross section (TCS). The TCS for BrU is found to be 2500 Mb and that for uracil is 1600 Mb showing an enhancement of 1.6 times for bromouracil. A similar enhancement factor was also reported for the iodouracil molecule in collisions with higher energy ion beams [19], as well as for double strand breaking in case of the Pt nanoparticle embedded in plasmid DNA [5].

5. Conclusions

We have presented the experimental and theoretical DDCS of the ejected electrons from the bromouracil and uracil molecules in collisions with protons of energy 200 keV. The measurements have been performed on a wide range of emission angles i.e. between 20° and 150°. The optimized structure of the bromouracil molecule was calculated along with a SCF density approach to estimate the population distribution. The

CDW-EIS model which includes the two center effect and PCI, underestimates the data for both the molecules. It can be inferred that these effects, at this low projectile energy, are too strong to be fully accounted by the model. This is the first time that the model has been extended for a most stringent collision condition i.e. for such large molecules as targets and the projectiles of intermediate velocity. A maximum enhancement in the electron emission from BrU by a factor of around 2 to 2.5 was observed in case of the large backward angles which is much higher than the prediction of the CDW-EIS model. The angular distribution of the DDCS ratios indicates a higher enhancement in the backward direction compared to the forward angles. The TCS obtained from the integrated DDCS over the emission energy and angle shows an enhancement by a factor of 1.6. We have also deduced the forward backward angular asymmetry parameter which was found to reveal a broad structure for uracil but not for the bromouracil. For bromouracil one obtains a lower asymmetry parameter having a smooth variation with electron energy as one obtains in ion-atom collisions. A suitable model is desirable to explain this feature. The large enhancement in case of bromouracil could be due to the Auger cascade phenomena or atomic giant resonance in Br atom. Since generation of low energy electrons is directly related to the breaking of strands of the DNA/RNA of cells, bromouracil can be tagged as a radiosensitizer.

Acknowledgments

The authors would like to acknowledge N Mhatre and S N Manjrekar for their help during the experiment. Support of the Department of Atomic Energy, Govt. of India, under Project No. 12P-R & D-TFR-5.02-0300 is acknowledged. Sandia National Laboratories is a multi-mission laboratory managed and operated by National Technology and Engineering Solutions of Sandia, LLC., a wholly owned subsidiary of Honeywell International, Inc., for the US Department of Energy's National Nuclear Security Administration under Contract DE-NA0003525. The views expressed in the article do not necessarily represent the views of the US DOE or the United States Government.

Data availability statement

The data that support the findings of this study are available upon reasonable request from the authors.

ORCID iDs

Juan M Monti https://orcid.org/0000-0002-8652-4600
Deepankar Misra https://orcid.org/0000-0001-6048-3444
Lokesh C Tribedi https://orcid.org/0000-0002-9282-9734

References

[1] Boudaiffa B, Cloutier P, Hunting D, Huels M A and Sanche L 2000 *Science* **287** 1658
[2] Schardt D, Elsässer T and Schulz-Ertner D 2010 *Rev. Mod. Phys.* **82** 383–425
[3] Begg A C, Stewart F A and Vens C 2011 *Nat. Rev. Cancer* **11** 239–53
[4] Verkhovtsev A V, Korol A V and Solov'yov A V 2015 *Phys. Rev. Lett.* **114** 063401
[5] Porcel E, Liehn S, Remita H, Usami N, Kobayashi K, Furusawa Y, Sech C L and Lacombe S 2010 *Nanotechnology* **21** 085103
[6] Butterworth K T, Wyer J A, Brennan-Fournet M, Latimer C J, Shah M B, Currell F J and Hirst D G 2008 *Radiat. Res.* **170** 381–7
[7] Fangxing X, Yi Z, Yunhui H, Cloutier P, Hunting D and Sanche L 2011 *Nanotechnology* **22** 465101
[8] McLaughlin P W, Mancini W R, Stetson P L, Greenberg H S, Nguyen N, Seabury H, Heidorn D B and Lawrence T S 1993 *Int. J. Radiat. Oncol. Biol. Phys.* **26** 637–42
[9] Kinsella T J, Dobson P P, Mitchell J B and Fornace A J 1987 *Int. J. Radiat. Oncol. Biol. Phys.* **13** 733–9
[10] Lawrence T S, Davis M A, Maybaum J, Stetson P L and Ensminger W D 1990 *Radiat. Res.* **123** 192–8
[11] Bacchus-Montabonel M C 2012 *Eur. Phys. J.* D **66** 175
[12] Itälä E, Ha D T, Kooser K, Rachlew E, Huels M A and Kukk E 2010 *J. Chem. Phys.* **133** 154316
[13] Champeaux J-P, Çarçabal P, Rabier J, Cafarelli P, Sence M and Moretto-Capelle P 2010 *Phys. Chem. Chem. Phys.* **12** 5454–61
[14] Delaunay R *et al* 2014 *Eur. Phys. J.* D **68** 162
[15] Castrovilli M C *et al* 2017 *Phys. Chem. Chem. Phys.* **19** 19807–14
[16] van der Burgt P J M, Brown M A, Bockova J, Rebelo A, Ryszka M, Poully J-C and Eden S 2019 *Eur. Phys. J.* D **73** 184
[17] Imhoff M, Deng Z and Huels M A 2007 *Int. J. Mass Spectrom.* **262** 154–60
[18] Abdoul-Carime H, Huels M A, Brüning F, Illenberger E and Sanche L 2000 *J. Chem. Phys.* **113** 2517–21
[19] Mandal A, Roy Chowdhury M, Bagdia C, Monti J M, Rivarola R D, Weck P F and Tribedi L C 2020 *Phys. Rev.* A **102** 062811
[20] Agnihotri A N *et al* 2013 *J. Phys. B: At. Mol. Opt. Phys.* **46** 185201
[21] Iriki Y, Kikuchi Y, Imai M and Itoh A 2011 *Phys. Rev.* A **84** 032704
[22] de Vera P, Garcia-Molina R, Abril I and Solov'yov A V 2013 *Phys. Rev. Lett.* **110** 148104

[23] Bhattacharjee S, Bagdia C, Roy Chowdhury M, Mandal A, Monti J M, Rivarola R D and Tribedi L C 2019 *Phys. Rev.* A **100** 012703
[24] Agnihotri A N, Nandi S, Kasthurirangan S, Kumar A, Galassi M E, Rivarola R D, Champion C and Tribedi L C 2013 *Phys. Rev.* A **87** 032716
[25] Itoh A, Iriki Y, Imai M, Champion C and Rivarola R D 2013 *Phys. Rev.* A **88** 052711
[26] Tabet J, Eden S, Feil S, Abdoul-Carime H, Farizon B, Farizon M, Ouaskit S and Mark T D 2010 *Phys. Rev.* A **82** 022703
[27] Moretto-Capelle P and Le Padellec A 2006 *Phys. Rev.* A **74** 062705
[28] Markush P *et al* 2016 *Phys. Chem. Chem. Phys.* **18** 16721–9
[29] Galassi M E, Champion C, Weck P F, Rivarola R D, Fojón O and Hanssen J 2012 *Phys. Med. Biol.* **57** 2081–99
[30] Winstead C and McKoy V 2006 *J. Chem. Phys.* **125** 174304
[31] Feil S *et al* 2004 *J. Phys. B: At. Mol. Opt. Phys.* **37** 3013–20
[32] Shafranyosh I I and Sukhoviya M I 2012 *J. Chem. Phys.* **137** 184303
[33] Verkhovtsev A, Traore A, Muñoz A, Blanco F and García G 2017 *Radiat. Phys. Chem.* **130** 371–8
[34] Padellec A L, Moretto-Capelle P, Richard-Viard M, Champeaux J P and Cafarelli P 2008 *J. Phys.: Conf. Ser.* **101** 012007
[35] Agnihotri A N, Kelkar A H, Kasthurirangan S, Thulasiram K V, Desai C A, Fernandez W A and Tribedi L C 2011 *Phys. Scr.* **T144** 014038
[36] Kasthurirangan S, Agnihotri A N, Desai C A and Tribedi L C 2012 *Rev. Sci. Instrum.* **83** 073111
[37] Mandal A and Tribedi L C 2019 *Nucl. Instrum. Methods Phys. Res.* B **440** 19–24
[38] Abdoul-Carime H, Huels M A, Brüning F, Illenberger E and Sanche L 2000 *J. Chem. Phys.* **113** 2517–21
[39] Fainstein P D, Ponce V H and Rivarola R D 1988 *J. Phys. B: At. Mol. Opt. Phys.* **21** 287–99
[40] Corchs S E, Rivarola R D and McGuire J H 1993 *Phys. Rev.* A **47** 3937–44
[41] Frisch M J *et al* 2009 *Gaussian 09 Revision A02* (Wallingford CT: Gaussian, Inc.)
[42] Lifschitz C, Bergmann E D and Pullman B 1967 *Tetrahedron Lett.* **8** 4583–6
[43] Palmer M H, Simpson I and Platenkamp R J 1980 *J. Mol. Struct.* **66** 243–63
[44] Stolterfoht N, DuBois R D and Rivarola R D 1997 *Electron Emission in Heavy Ion-Atom Collisions* (Berlin: Springer)
[45] Hikosaka Y, Lablanquie P, Kaneyasu T, Adachi J, Tanaka H, Suzuki I H, Ishikawa M and Odagiri T 2021 *J. Phys. B: At. Mol. Opt. Phys.* **54** 185002
[46] Hikosaka Y, Lablanquie P, Kaneyasu T, Adachi J, Tanaka H, Suzuki I H, Ishikawa M and Odagiri T 2021 *Phys. Rev.* A **103** 043119
[47] Hu Z, Caló A, Nikkinen J, Matila T, Kukk E, Aksela H and Aksela S 2004 *J. Chem. Phys.* **121** 8246–52
[48] Amusia M Y, Chernysheva L V, Felfli Z and Msezane A Z 2001 *Phys. Rev.* A **64** 032711
[49] Boo B H and Saito N 2003 *J. Electron Spectrosc. Relat. Phenom.* **128** 33–44
[50] Fainstein P D, Gulyás L, Martín F and Salin A 1996 *Phys. Rev.* A **53** 3243–6